

**AD-A256 458**



## The Influence of Steel Surface Chemistry on the Bonding of Lubricant Films

Prepared by

S. V. DIDZIULIS, M. R. HILTON, and P. D. FLEISCHAUER  
Mechanics and Materials Technology Center  
Technology Operations

1 September 1992

Prepared for

SPACE AND MISSILE SYSTEMS CENTER  
AIR FORCE MATERIEL COMMAND  
Los Angeles Air Force Base  
P. O. Box 92960  
Los Angeles, CA 90009-2960

Engineering and Technology Group

THE AEROSPACE CORPORATION  
El Segundo, California

APPROVED FOR PUBLIC RELEASE;  
DISTRIBUTION UNLIMITED

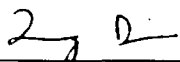
**92-27650**



This report was submitted by The Aerospace Corporation, El Segundo, CA 90245-4691, under Contract No. F04701-88-C-0089 with the Space and Missile Systems Center, P. O. Box 92960, Los Angeles, CA 90009-2960. It was reviewed and approved for The Aerospace Corporation by R. W. Fillers, Principal Director, Mechanics and Materials Technology Center. Capt Mark Borden was the project officer for the Mission-Oriented Investigation and Experimentation (MOIE) program.

This report has been reviewed by the Public Affairs Office (PAS) and is releasable to the National Technical Information Service (NTIS). At NTIS, it will be available to the general public, including foreign nationals.

This technical report has been reviewed and is approved for publication. Publication of this report does not constitute Air Force approval of the report's findings or conclusions. It is published only for the exchange and stimulation of ideas.



---

QUANG BUI, Lt, USAF  
MOIE Program Manager



---

MARK W. BORDEN, Capt, USAF  
SSUSI/SSULI Project Officer  
DMSP Program Office

UNCLASSIFIED

SECURITY CLASSIFICATION OF THIS PAGE

## REPORT DOCUMENTATION PAGE

1a. REPORT SECURITY CLASSIFICATION <b>Unclassified</b>			1b. RESTRICTIVE MARKINGS		
2a. SECURITY CLASSIFICATION AUTHORITY			3. DISTRIBUTION/AVAILABILITY OF REPORT  Approved for public release; distribution unlimited		
2b. DECLASSIFICATION/DOWNGRADING SCHEDULE					
4. PERFORMING ORGANIZATION REPORT NUMBER(S) <b>TR-0091(6945-03)-5</b>			5. MONITORING ORGANIZATION REPORT NUMBER(S) <b>SMC-TR-92-38</b>		
6a. NAME OF PERFORMING ORGANIZATION <b>The Aerospace Corporation Technology Operations</b>		6b. OFFICE SYMBOL (If applicable)	7a. NAME OF MONITORING ORGANIZATION <b>Space and Missile Systems Center</b>		
6c. ADDRESS (City, State, and ZIP Code) <b>El Segundo, CA 90245-4691</b>			7b. ADDRESS (City, State, and ZIP Code) <b>Los Angeles Air Force Base Los Angeles, CA 90009-2960</b>		
8a. NAME OF FUNDING/SPONSORING ORGANIZATION		8b. OFFICE SYMBOL (If applicable)	9. PROCUREMENT INSTRUMENT IDENTIFICATION NUMBER <b>F04701-88-C-0089</b>		
8c. ADDRESS (City, State, and ZIP Code)			10. SOURCE OF FUNDING NUMBERS		
			PROGRAM ELEMENT NO.	PROJECT NO.	TASK NO.
			WORK UNIT ACCESSION NO.		
11. TITLE (Include Security Classification)  <b>The Influence of Steel Surface Chemistry on the Bonding of Lubricant Films</b>					
12. PERSONAL AUTHOR(S) <b>Didziulis, Stephen V; Hilton, Michael R.; and Fleischauer, Paul D.</b>					
13a. TYPE OF REPORT		13b. TIME COVERED FROM _____ TO _____		14. DATE OF REPORT (Year, Month, Day) <b>1992, September 1</b>	
				15. PAGE COUNT <b>22</b>	
16. SUPPLEMENTARY NOTATION					
17. COSATI CODES			18. SUBJECT TERMS (Continue on reverse if necessary and identify by block number)		
FIELD	GROUP	SUB-GROUP			
			Extreme Pressure Additive		
			440C Stainless Steel		
			Lead Naphthenate		
			Molybdenum Disulfide		
			Solid Lubrication		
			Surface Chemistry		
19. ABSTRACT (Continue on reverse if necessary and identify by block number) Virtually all moving mechanical assemblies on spacecraft contain steel components that must be effectively lubricated to ensure optimum performance and long life. This report details the surface chemical composition of 440C stainless steel and its interaction with two lubricant species: the solid lubricant MoS <sub>2</sub> and the liquid lubricant extreme pressure (EP) additive, lead naphthenate (Pbnp). X-ray photoelectron spectroscopy (XPS) studies show that the 440C surface has a layered oxide structure following polishing and solvent cleaning; a 2.5 nm thick iron oxide layer exists on top of a thinner 1.5 nm chromium oxide underlayer. A region of high metal carbide concentration is present at the chromium oxide-bulk steel interface. Therefore, a layer of iron oxide (not the corrosion barrier formed by the chromium oxide layer) is the top surface layer with which lubricant species interact under conditions of low stress. The surface chemical composition of 440C can be altered by chemical or physical means. Chemical treatments such as acidic and alkaline etches selectively remove the iron oxide overlayer, leaving behind a surface enriched in chromium oxide. Furthermore, the alkaline treatment proved to be more controllable, while the acid treatment can cause surface damage by breaking through the corrosion barrier and severely oxidizing the bulk steel. The oxide layers can also be removed by Ar <sup>+</sup> ion sputtering, but this treatment					
20. DISTRIBUTION/AVAILABILITY OF ABSTRACT <input checked="" type="checkbox"/> UNCLASSIFIED/UNLIMITED <input type="checkbox"/> SAME AS RPT. <input type="checkbox"/> DTIC USERS				21. ABSTRACT SECURITY CLASSIFICATION <b>Unclassified</b>	
22a. NAME OF RESPONSIBLE INDIVIDUAL			22b. TELEPHONE (Include Area Code)		22c. OFFICE SYMBOL

UNCLASSIFIED

is not as selective as the chemical treatments, since some of the iron oxide overlayer is chemically reduced to iron metal in addition to being sputtered away.

Thin (1  $\mu\text{m}$ )  $\text{MoS}_2$  films were radio frequency sputter deposited onto 440C substrates, following the different chemical treatments. The adhesion of the films to the steel was enhanced by both the acid and base pretreatments, which should lead to better performance of the lubricant. The Pbnp molecule also had significantly different chemical reactions with the steel surface, following the removal of the oxide layer(s). The breakdown of Pbnp to metallic Pb was observed to occur when the Pbnp molecule interacts with metallic species in the steel that are exposed by scratching the surface or after acid etching. The formation of metallic lead (which can act as a solid lubricant) at high temperatures in the presence of metallic species provides insight into the mechanism by which the additive provides protection under EP conditions. This work shows that steel surface chemistry plays a pivotal role in the bonding of lubricant films and that this interaction can be altered by changing the steel surface composition. The tribological implications of these chemical changes are currently being investigated.

## PREFACE

The authors thank R. Bauer and J. Childs of The Aerospace Corporation for experimental assistance.

Approved For	
Name _____	X
Date _____	SJ
By _____	
Title _____	
Special Agent in Charge	
Dit _____	
A-1	

100-443887-100

## CONTENTS

PREFACE .....	1
I. INTRODUCTION .....	5
II. EXPERIMENTAL SECTION .....	7
III. XPS RESULTS AND DISCUSSION .....	9
A. XPS Sputter Profile .....	9
B. Angle Resolved XPS .....	11
C. Chemical Treatments of 440C .....	12
D. Interaction of 440C with Lubricant Films .....	14
IV. CONCLUSIONS .....	19
REFERENCES .....	21

## FIGURES

1. (a) An XPS sputter profile of a solvent cleaned 440C surface with an accompanying diagram showing the layered oxide structure of the surface region; (b) The Cr and Fe 2p <sub>3/2</sub> peaks as a function of sample angle $\phi$ from equation 1 .....	10
2. The (a) Fe 2p <sub>3/2</sub> and (b) Cr 2p <sub>3/2</sub> XPS peaks as a function of the sample treatments listed on the figure .....	13
3. Two magnifications of SEM micrographs of the Rockwell indentations performed on the MoS <sub>2</sub> films deposited on differently treated 440C .....	15
4. The (a) Pb 4f <sub>7/2,5/2</sub> and (b) C 1s XPS peaks of several Pbnp treated 440C samples .....	17
5. The Pb 4f XPS peaks of Pbnp treated 440C as a function of the sample heating temperatures listed on the figure .....	18

## I. INTRODUCTION

The preponderance of mechanical assemblies manufactured from steels makes the lubrication of steel component surfaces the predominant problem in the field of tribology. In certain situations, such as the use of solid lubricants and boundary additives in liquid lubricants, the steel surface chemistry must play an intimate role in determining the success or failure of the lubricant. In particular, understanding the adhesion of solid lubricant films to components and the performance of extreme pressure (EP) oil additives operating under boundary conditions requires knowledge concerning the chemical composition and reactivity of the steel surface under study. In this report, the chemical composition of the surface region of AISI 440C steel was explored with X-ray photoelectron spectroscopy (XPS) in order to determine the roles of the various surface species in interactions with radio frequency (rf) sputtered molybdenum disulfide ( $\text{MoS}_2$ ) solid lubricant films and with the EP oil additive lead naphthenate (Pbnp).

Steel surface chemistry has been the subject of substantial amounts of experimental work (Ref. 1). High chromium stainless steels (such as 440C) generally show segregation of chromium to the surface region; a corrosion barrier is obtained once a chromium oxide layer has formed (Ref. 2). In this work, detailed XPS studies of the oxide structure of 440C are presented, along with data examining the effects of chemical treatments on the surface composition. Finally, the effects of changing the steel surface composition on the adhesion and growth of  $\text{MoS}_2$  films and the bonding interactions of Pbnp are also reported.

The two lubricant materials used in this work,  $\text{MoS}_2$  and Pbnp, have chemical bonding and reactivity properties which enhance their tribological performance. The lubricating properties of  $\text{MoS}_2$  result from its anisotropic, layered structure (Ref. 3). The material forms sandwiches of S-Mo-S having very strong Mo-S bonds, but only weak van der Waals interactions exist between sulfur layers of adjacent sandwiches. The weak van der Waals interactions result in very low shear strength perpendicular to the  $\text{MoS}_2$  c-axis and produce highly inert, S-terminated (0001) basal planes (Ref. 4). The adhesion and growth of sputter deposited  $\text{MoS}_2$  films are also affected by this structure, with reactive edge plane atoms acting as nucleation sites for faster film growth (Ref. 5). Pbnp provides decreased wear and low friction for steel surfaces operating under EP conditions of metal-to-metal contact and high temperature. The method by which Pbnp provides protection is unknown, but interaction with the steel surface must take place, leading to adsorption and/or reaction on the steel, for boundary protection to occur. The principal surface analysis technique employed in this work is XPS, which gives both quantitative surface composition information from peak intensities and qualitative information regarding the oxidation state and bonding environments of surface species from the binding energy positions of peaks.

## II. EXPERIMENTAL SECTION

Samples of AISI 440C steel were cut into coupons approximately  $6 \times 6 \times 2$  mm in size. The samples were polished with slurries of alumina in water down to  $0.05 \mu\text{m}$  grit size, cleaned in ethanol, and stored in a nitrogen purged desiccator until needed. Before introduction into the surface analysis vacuum system or deposition of lubricant species, the steel samples were subjected to a variety of chemical treatments while being agitated in an ultrasonic cleaner. Some samples were simply cleaned once again with ethanol. Others were subjected to acid etches for 30 s in a 20% concentrated HCl/ethanol solution followed by several ethanol rinses. Additional samples were cleaned for 1 h in a commercial, buffered alkaline solution (Alum Etch 34), ~15% in deionized water (pH = 12.8), followed by a brief rinse with deionized water and ultrasonic cleaning in ethanol. All treatments were conducted in the laboratory ambient; exposure to air was limited by keeping samples immersed in ethanol following treatments.

Thin films of  $\text{MoS}_2$  were deposited onto the steel substrates in an rf sputtering system, which has been described elsewhere (Ref. 6). The steel coupons were placed in the diffusion pumped deposition system following chemical treatment and pumped down overnight (base pressure  $1 \times 10^{-6}$  Torr). The  $1\text{-}\mu\text{m}$ -thick films were produced at a deposition rate of  $27.5 \text{ nm/min}$ , with the sample temperature floating and reaching a maximum of  $70^\circ\text{C}$ .  $\text{MoS}_2$  film structure and adhesion were studied by fracturing the film with a diamond brale indenter ( $200 \mu\text{m}$  radius of curvature) in a Rockwell hardness tester (150 kg load), followed by analysis with scanning electron microscopy (SEM) in a Cambridge Stereoscan S-200. The details of this procedure are outlined elsewhere (Ref. 7).

The steel surfaces were exposed to Pbnp by immersing the differently pretreated coupons into a 1–2 g/L solution of Pbnp in heptane for 1 min. During immersion, areas of the samples (approximately  $2 \times 2 \text{ mm}$ ) were scratched with a diamond scribe with sufficient force to plastically deform the surfaces to a depth of 1 to  $2 \mu\text{m}$  as determined by surface profilometry. The scratching procedure was pursued in order to expose bulk steel to the Pbnp solution by breaking through the thin oxide layers. Following immersion, the samples were rinsed with heptane and immersed in ethanol. Prior to introduction into the ultrahigh vacuum (UHV) system for XPS analysis, the samples were exposed to air for approximately 5 min during mounting.

The surface composition of the treated steel surfaces and the chemical reaction of Pbnp on steel were studied with a Surface Science Instruments (SSI) SSX-100 XPS system. The UHV system (base pressure  $< 1 \times 10^{-10}$  Torr) and instrument have been described elsewhere (Ref. 8). The  $300\text{-}\mu\text{m}$  spot size from the monochromatized Al  $\text{K}\alpha$  anode and 50-eV pass energy used for this study produce a Au  $4f_{7/2}$  peak at  $84.0 \text{ eV}$  with a full-width-at-half-maximum of  $0.95 \text{ eV}$ . All binding energies are referenced to the spectrometer Fermi level. Data were obtained with the sample normal tilted by  $60^\circ$  relative to the central axis of the electron energy analyzer, unless otherwise stated. An XPS sputter profile of a solvent cleaned 440C surface was performed with  $2 \text{ keV Ar}^+$  ions to study the oxide layer structure. Spectra were obtained on the unscratched and scratched regions of the Pbnp exposed samples. The Pbnp treated



samples were also heated in the UHV system to simulate temperature increases expected during boundary contact.

### III. XPS RESULTS AND DISCUSSION

#### A. XPS SPUTTER PROFILE

Figure 1 presents two different methods for determining the oxide layer structure on solvent cleaned 440C. Figure 1(a) is an XPS sputter profile, giving atomic concentrations assuming a homogeneous sample as a function of sputter time. The profile shows four different regions, separated by dashed lines, to exist on the 440C sample. Before sputtering, a strong carbon peak having a binding energy near 285 eV is evident, along with the Fe, Cr, and O signals expected for an oxidized steel surface. Both the characteristic C 1s binding energy and its rapid removal with sputtering ( $< 1$  min) indicate that the surface is contaminated with a layer of hydrocarbons. From 1 to 6 min of sputter time, the O signal decreases linearly while the Fe intensity remains about constant and the Cr signal increases. During this sputtering period, the Fe 2p XPS peaks show a monotonic decrease in the signal associated with iron oxide species (primarily  $\text{Fe}_2\text{O}_3$ ) relative to the metallic iron signal. In addition, both the chromium oxide and chromium metal peaks increase in intensity, maintaining the same relative oxide-to-metal peak intensities. This behavior is consistent with the removal and possible chemical reduction of a layer of iron oxides, leading to an increase in the intensities of underlying species [metallic iron, chromium oxides, and metallic chromium (Ref. 9)]. In the 6 to 9–10 min sputter time frame, the oxygen signal decreases sharply, while the iron signal increases sharply and chromium shows a slight decline. The Cr 2p XPS peaks show that chromium oxides (primarily  $\text{Cr}_2\text{O}_3$ ) are being sputtered away, eventually leaving behind a surface that is quite similar in composition (72% Fe, 18% Cr, 8% C, 2% O) to the bulk steel. A diagram of the steel surface region is given above the sputter profile, including oxide thicknesses determined by the calibration of the  $\text{Ar}^+$  ion etch rate (0.42 nm/min) with an  $\text{SiO}_2/\text{Si}$  sample of known oxide thickness.

The abrupt changes in the slopes of the surface composition profile and the peak shape changes observed in the Fe and Cr core levels with sputtering are a direct result of the layered oxide surface structure on 440C. If the surface region were composed of mixed iron and chromium oxides or gradually changing compositions (graded interface), then much more gradual changes would have been observed. In fact, it is difficult to support the existence of anything but a layered oxide structure with fairly sharp boundaries between the metal and chromium oxide layer and between the two oxide layers based on this data. Only a very small amount of iron oxide intensity is evident during the early stages (first minute) of sputtering through the chromium oxide underlayer. While this signal could be taken as proof of the existence of some interfacial mixing of the oxides, it could also be explained by surface roughness effects, by knock-on effects, or by the existence of a small amount of an interfacial iron-chromium oxide spinel compound which has been proposed to exist (Ref. 10).

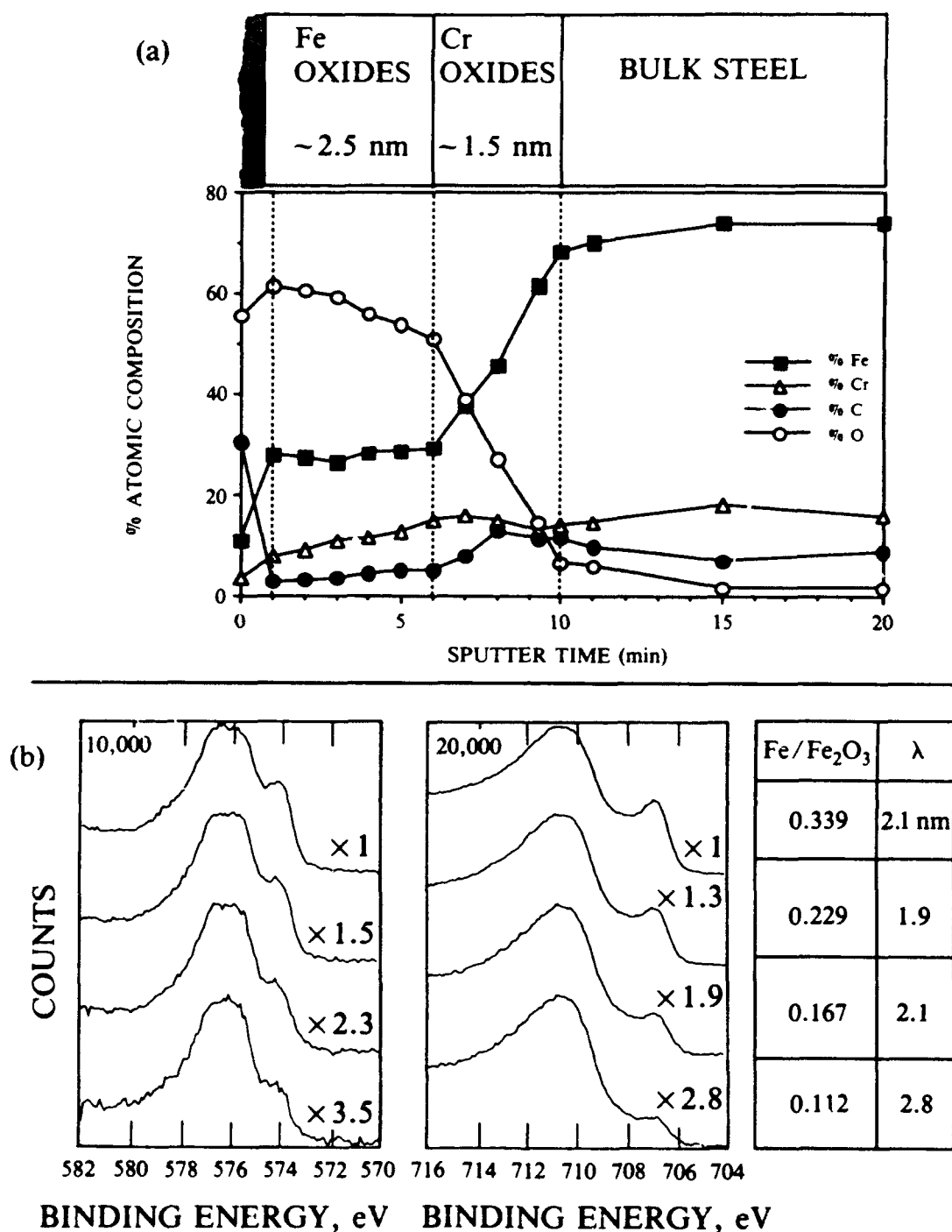


Figure 1. (a) An XPS sputter profile of a solvent cleaned 440C surface with an accompanying diagram showing the layered oxide structure of the surface region. (b) The Cr (left) and Fe  $2p_{3/2}$  peaks as a function of sample angle  $\phi$  from equation 1. From the top, the angles between the surface normal and the electron analyzer entrance cone are  $0^\circ$ ,  $20^\circ$ ,  $40^\circ$  and  $60^\circ$ . The table at the right gives the experimental Fe/Fe<sub>2</sub>O<sub>3</sub> intensity ratios and the calculated electron escape depths.

## B. ANGLE RESOLVED XPS

Figure 1(b) gives the Cr 2p<sub>3/2</sub> and the Fe 2p<sub>3/2</sub> core levels obtained as a function of sample angle relative to the central axis of the electron energy analyzer. Moving down the figure, the sample normal has been tilted away from the analyzer, decreasing the effective escape depth of the electrons from the material and increasing the surface sensitivity of the technique. This angular effect allows the relative positions and thicknesses of layers in a material to be determined without destroying the interface with ion sputtering. The data in Figure 1(b) are normalized to the intensities of the higher binding energy iron and chromium oxide features and show that rotating the sample away from the analyzer increases the intensities of both the iron and chromium oxides relative to the metal signals. This result proves that the oxides exist on top of the metallic species. In addition, the decreasing effective escape depth has a greater impact on the absolute chromium oxide signal intensities than on the iron oxide features, as indicated by the greater normalization factors listed for the Cr spectra on the figure. This result shows that the chromium oxides are deeper into the bulk of the sample than the iron oxides, in agreement with the sputter profile.

The angular intensity effects can be quantified for comparison to the sputter profile results just discussed. Equations used to study the attenuation of substrate XPS peaks by an overlayer (Ref. 11) can be readily modified for the duplex overlayers present on 440 C, as shown in equation 1.

$$\frac{I_{\text{Fe}}}{I_{\text{Fe}_2\text{O}_3}} = \frac{I_{\text{Fe}}^0 e^{\left(\frac{-(x+y)}{\lambda \cos \phi}\right)}}{I_{\text{Fe}_2\text{O}_3}^0 \left[ 1 - e^{\left(\frac{-x}{\lambda \cos \phi}\right)} \right]} \quad (1)$$

In equation 1,  $I_{\text{Fe}}$  and  $I_{\text{Fe}_2\text{O}_3}$  are the integrated XPS intensities of the iron metal and iron oxide components of the Fe 2p<sub>3/2</sub> spectrum, respectively; the  $I^0$ 's are the intensities expected for single component systems;  $x$  ( $y$ ) is the thickness of the iron (chromium) oxide overlayer;  $\lambda$  is the photoelectron scattering length in the oxide overlayer; and  $\phi$  is the angle between the surface normal and the analyzer axis. The value of  $\lambda$  is assumed to be the same in both oxide layers. The  $I^0$  ratio [ $I^0(\text{Fe})/I^0(\text{Fe}_2\text{O}_3)$ ] is calculated to be 1.57 from the relative Fe atomic densities in 440C steel and Fe<sub>2</sub>O<sub>3</sub>, assuming the photoionization cross sections of the two iron species to be the same.

In order for equation 1 to be used, a value for  $\lambda$  must be determined for a Fe 2p photoelectron with a kinetic energy of ~780 eV. There are methods for calculating  $\lambda$  (Ref. 12), but their veracity is still a matter of conjecture, especially for a complex, multiphase material such as 440C. Instead, we will use the oxide thickness values determined by the sputter profile to calculate a value for  $\lambda$  from equation 1. (The oxide thicknesses determined by the sputter profile could be in error if the sputtering rates of the metal oxides are significantly different than that for the calibration sample.) The total oxide thickness ( $d$ ) was determined to be 3.8–4.4 nm, with the iron oxide ( $x$ ) 2.3–2.7 nm and the chromium oxide ( $y$ ) 1.3–1.7 nm thick. Experimental

peak intensities were determined by fitting the data with the SSI data analysis software using Gaussian broadened Lorentzian peaks and a Shirley background; the Fe/Fe<sub>2</sub>O<sub>3</sub> integrated intensity ratios are given in Figure 1. The  $\lambda$  values obtained from equation 1 at the four different angles with  $x = 2.5$  nm and  $y = 1.5$  nm (also given next to the Fe spectra in Figure 1) are fairly consistent and result in an average value of 2.2 nm. This  $\lambda$  is reasonable for 780 eV electrons but slightly larger than expected when compared to values obtained from the "universal curve" of electron mean free paths (Ref. 13). The larger  $\lambda$  could be the result of inhomogeneous oxide thicknesses due to surface roughness effects, as the calculated value of  $\lambda$  is greatest at the largest angle [Figure 1(b)].

### C. CHEMICAL TREATMENTS OF 440C

The effects of chemical treatments on the steel surface composition are shown in Figure 2, which compares the Fe and Cr 2p<sub>3/2</sub> peaks following the specified treatment. The most significant changes are observed in the Fe data, which show a large decrease in the amount of surface iron oxides following both the acid etch and the alkaline wash. In contrast, the Cr peaks show little change in the oxide:metal relative intensities. The total Fe/total Cr peak intensity ratios decrease greatly from typical values of 3.2 for the solvent cleaned samples to values ranging from 1.3 to 2.0 for the acid and base treated steel. These results lead to a clear conclusion: the chemical treatments selectively remove the iron oxide overlayer, leaving behind a surface enriched in chromium oxides. In addition, the chemical treatments are more effective at selectively removing the iron oxide layer than ion sputtering, where the smallest Fe/Cr ratio was 2.1 after the sixth minute of sputtering. This result likely confirms that ion bombardment chemically reduces some of the Fe<sub>2</sub>O<sub>3</sub> to metallic iron in addition to removing material, causing a larger-than-expected value of Fe/Cr. Acid etched samples sometimes took on a milky appearance following the treatment, indicative of surface damage. If the samples were etched longer than 30 s, an increase in the amount of surface iron oxide was detected by XPS, showing that the acid had etched through the chromium oxide layer, initiating corrosion of the bulk steel (Ref. 9). Surface profilometry of acid etched surfaces indicated that samples etched for 0 to 30 s had average surface roughness of ~6 nm, while a 60 s etch had an average roughness of ~17 nm.

The effectiveness of the chemical treatments can be investigated through intensity analyses of the Fe/Cr ratios. If all of the iron oxide overlayer has been removed, these intensity ratios should be defined by equation 2.

$$\frac{I_{Fe}^{Metal}}{I_{Cr}^{Total}} = \frac{I_{Fe}^0 e^{\left(\frac{-y}{\lambda_{Fe} \cos \phi}\right)}}{I_{Cr_2O_3}^0 \left[ 1 - e^{\left(\frac{-y}{\lambda_{Cr} \cos \phi}\right)} \right] + I_{Cr}^0 e^{\left(\frac{-y}{\lambda_{Cr} \cos \phi}\right)}} \quad (2)$$

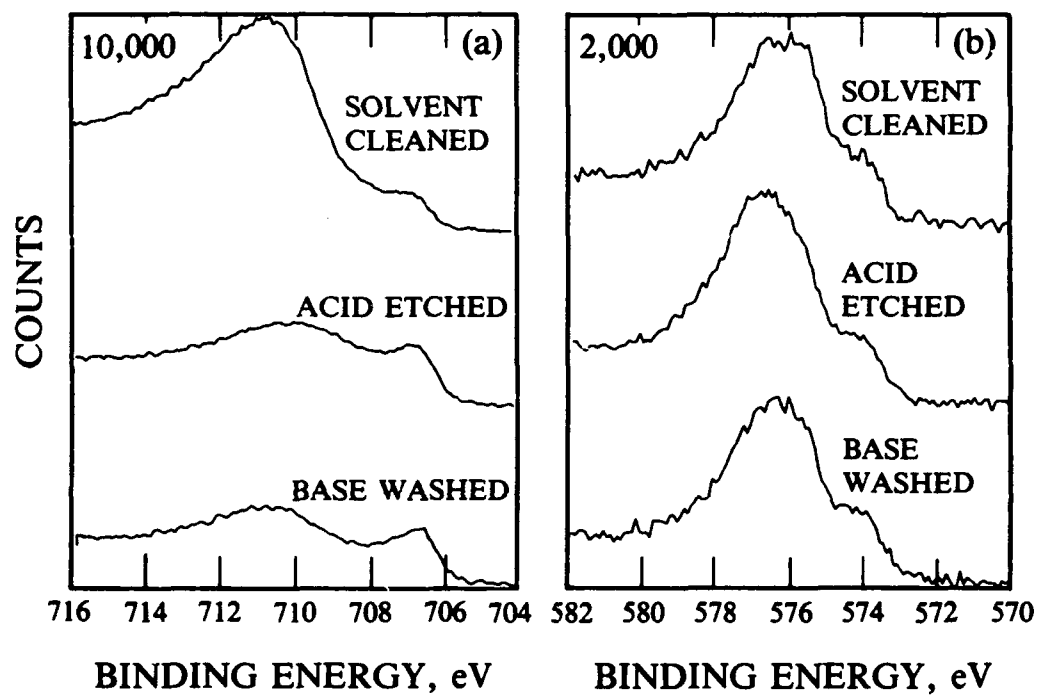


Figure 2. The (a) Fe 2p<sub>3/2</sub> and (b) Cr 2p<sub>3/2</sub> XPS peaks as a function of the sample treatments listed on the figure.

Values for the  $I^0$ 's must take into account the different metal atom densities in the various materials and the different Fe 2p and Cr 2p photoionization cross sections (Ref. 14). If some simplifying assumptions are made, setting  $\lambda_{\text{Fe}} = \lambda_{\text{Cr}} = 2.2 \text{ nm}$  and  $y = \lambda \cos \phi$ , then a Fe/Cr ratio of 1.3 is obtained. This Fe/Cr value is close to the range obtained after the chemical treatments (1.3 to 2.0), lending credence to this approach. More accurately, the slightly larger  $\lambda_{\text{Cr}}$  (for photoelectrons having kinetic energies of 910 eV) and the greater thickness of the  $\text{Cr}_2\text{O}_3$  layer ( $1.5 \text{ nm} > \lambda \cos \phi$  for  $\phi = 60^\circ$ ) would tend to lower this ratio. For example, if  $\lambda_{\text{Cr}} = 2.5 \text{ nm}$  and  $y = 1.5 \text{ nm}$ , then the calculated intensity ratio becomes 0.87. In our experiments, some iron oxide signal remains after all chemical treatments, resulting in Fe/Cr ratios in excess of this lower bound. The lowest experimental Fe/Cr ratios were obtained after alkaline washes (1.3 to 1.7), showing that this treatment was the most effective at selectively removing the iron oxide overlayer. Samples treated with the acid solution had a range of Fe/Cr ratios of 1.3 to 2.0. The acid etch data presented in Figure 2 shows the most selective iron oxide removal for any of the samples treated with this solution in this study (i.e., Fe/Cr = 1.3). As indicated above, most of the acid etched samples had higher Fe/Cr ratios than the alkaline washed samples.

The selective removal of iron oxide by the chemical treatments gives further support for the layered oxide structure indicated by the XPS results. The fact that some iron oxide signal remains after all sample treatments might support the existence of a small amount of an iron-chromium oxide compound that is not affected by the chemical treatments.

#### D. INTERACTION OF 440C WITH LUBRICANT FILMS

The effects of the chemical pretreatments on the adhesion of the rf-sputtered  $\text{MoS}_2$  films deposited on 440C are shown in Figure 3. The SEM micrographs presented in this figure show the extent of delamination around the Rockwell indentations. Qualitatively, it is obvious that the removal of the iron oxide overlayer by the acid and base treatments improves the fracture toughness and probably enhances the adhesion of the  $\text{MoS}_2$  film. Similar enhancements of adhesion are observed if the steel substrate is  $\text{Ar}^+$  ion cleaned in the sputter system prior to film deposition (Ref. 9). In addition, higher magnification micrographs indicate that the films deposited on the chemically treated surfaces appear slightly denser than on a solvent cleaned 440C surface. In previous work, denser  $\text{MoS}_2$  films of a given microstructure had a greater tendency to delaminate because of their reduced ability to blunt crack propagation due to decreased film porosity (Ref. 15). Although these results do not conclusively indicate that the  $\text{MoS}_2$  film has stronger bonding interactions with the chromium oxide components of the steel, the effects of the chemical pretreatments on film nucleation and adhesion indicate that more active sites for crystallite nucleation and strong adhesion exist on the steel surfaces after the chemical treatments. This result implies that the effect is dominantly chemical in nature. An increase in surface roughness could conceivably cause an increase in adhesion based on mechanical interlocking effects, but the samples used in this work displayed little change in surface roughness following sample treatment. In previous work, no enhancement in  $\text{MoS}_2$

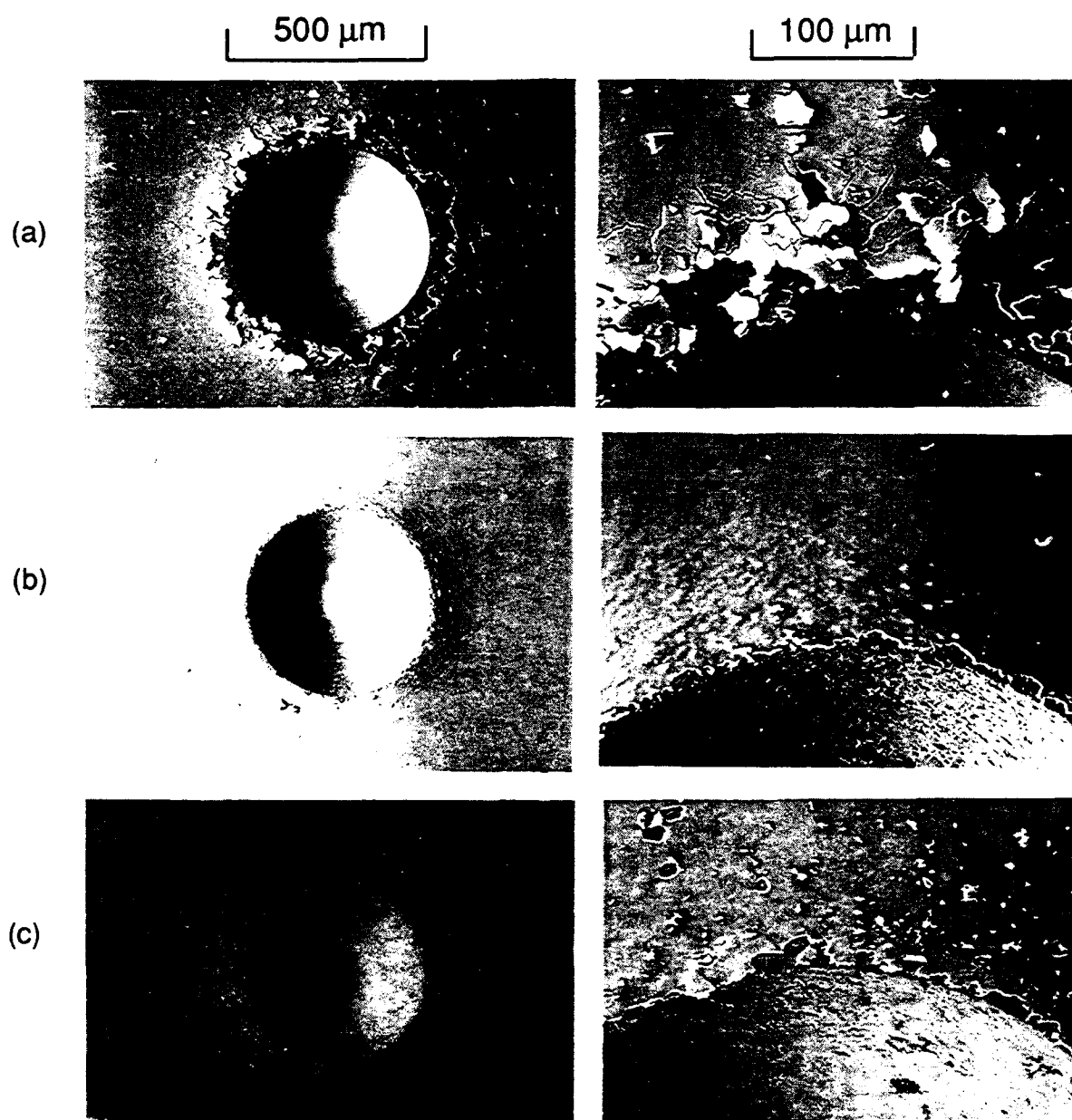


Figure 3. Two magnifications of SEM micrographs of the Rockwell indentations performed on the  $\text{MoS}_2$  films deposited on differently treated 440C. The treatments were (a) solvent cleaning, (b) acid etching, and (c) base washing.



adhesion was observed for 440C surfaces etched for 60 s relative to a 30 s etch sample despite a large increase in the measured surface roughness (Ref. 9). We conclude, therefore, that the enhanced adhesion is predominantly chemical in nature.

The final area of study to be discussed is the interaction of the EP additive Pbnp with the steel surfaces. The Pbnp molecule consists of cyclopentane terminated hydrocarbon chains of varying length bonded to a central Pb ion through the oxygen atoms of a carboxylate group. Figure 4 shows the Pb 4f and C 1s peaks obtained from Pbnp treated 440C surfaces as a function of sample pretreatment. On the solvent cleaned surface (1), the Pb 4f<sub>7/2</sub> peak has a binding energy of 139.2 eV, which has been identified as the binding energy for molecular Pbnp (Ref. 16). The C 1s spectrum from this same surface is quite complex, with a small peak near 283 eV from steel carbides, strong features near 285 and 286 eV, binding energies characteristic of hydrocarbons both in the naphthenate chain and as impurities, and a peak near 289 eV. The 289 eV binding energy is characteristic of the carboxylate carbon species expected for molecular Pbnp. Therefore, the strong carboxylate peak and the 139.2 eV Pb 4f<sub>7/2</sub> binding energy show that Pbnp is molecularly adsorbed (physisorbed) on iron oxide (Ref. 17).

The Pb and C XPS peaks obtained from the scratched area of the solvent cleaned sample (2) as well as the unscratched areas of the acid (3) and base treated (4) 440C samples are also included on Figure 4. For all of the altered surfaces, the Pb 4f<sub>7/2</sub> peak is shifted to lower binding energy by 0.3 to 0.4 eV, and the carboxylate C peak intensity is much weaker compared to solvent cleaned 440C. These changes indicate a different chemical interaction of Pbnp with the steel has occurred. The spectroscopic changes are consistent with partial breakdown of Pbnp through the breaking of the C-O bonds in the carboxylate group. The resulting Pb binding energy is not consistent with any forms of lead oxide and, coupled with the remaining carboxylate intensity, indicates that the chromium oxide species exposed by the chemical treatments and the metals exposed to the Pbnp solution during the scratching process are chemisorbing part of the Pbnp molecule.

Figure 5 shows the Pb 4f peaks from several Pbnp treated steel surfaces as a function of temperature. The solvent cleaned sample (a) loses most of its Pb signal on heating in UHV, indicating desorption of the Pbnp. The remaining Pb intensity shifts to two lower binding energy species, indicating some chemisorbed Pbnp (138.8 eV) and the formation of metallic lead (136.6 eV). In contrast, the scratched region of this surface (b) retained most of its Pb as metallic lead. Both the acid etched (c) and base washed (d) surfaces retained some metallic lead and chemisorbed Pbnp after heating. The reaction to metallic Pb, however, occurs at a lower temperature on the acid etched surface, and this surface also retains more total Pb than the base treated surface. In fact, other alkaline washed samples that had lower Fe/Cr ratios than the sample from which spectra are shown in Figure 5 retained no measurable amount of Pb. The steel surface composition also changes with heating, with metallic iron emerging with increasing temperature. The reaction of Pbnp to metallic Pb is strongly correlated to the emergence of metallic Fe (Ref. 17). This suggests that Pbnp reacts with metallic Fe under EP conditions to provide a layer of metallic lead that acts as a solid boundary lubricant.

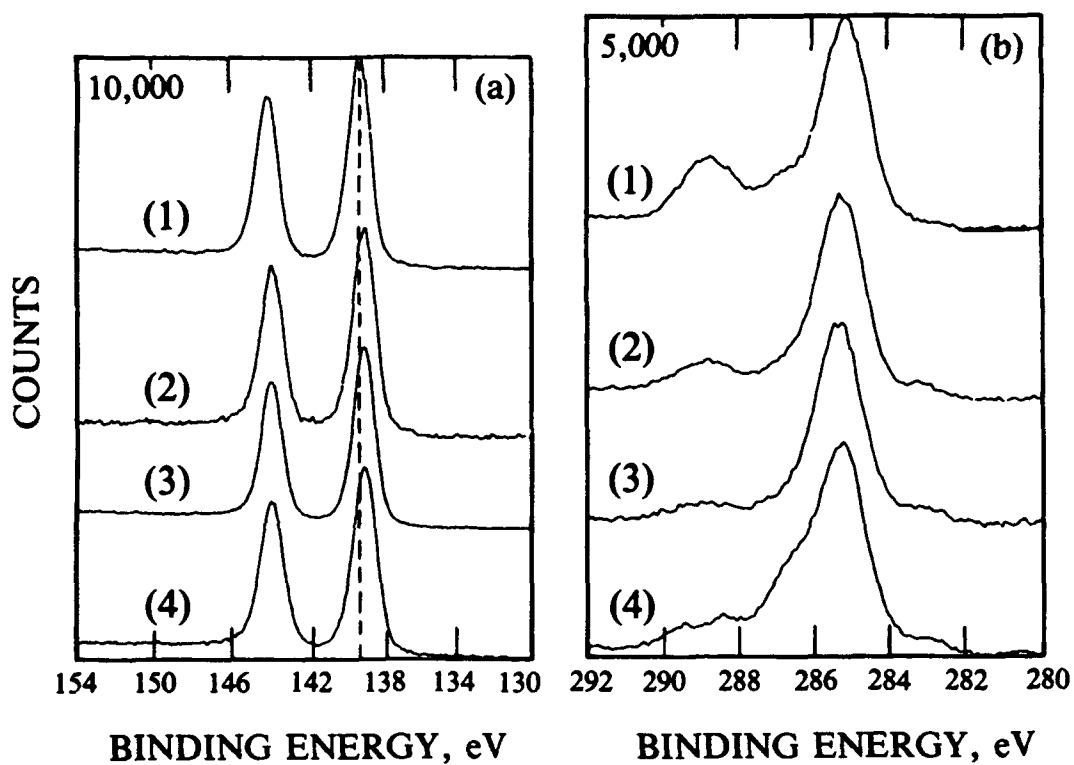


Figure 4. The (a) Pb 4f<sub>7/2</sub>, 5/2 and (b) C 1s XPS peaks of several Pbnp treated 440C samples. The samples are: (1) solvent cleaned, unscratched; (2) solvent cleaned, scratched; (3) acid etched, unscratched; and (4) base washed, unscratched.

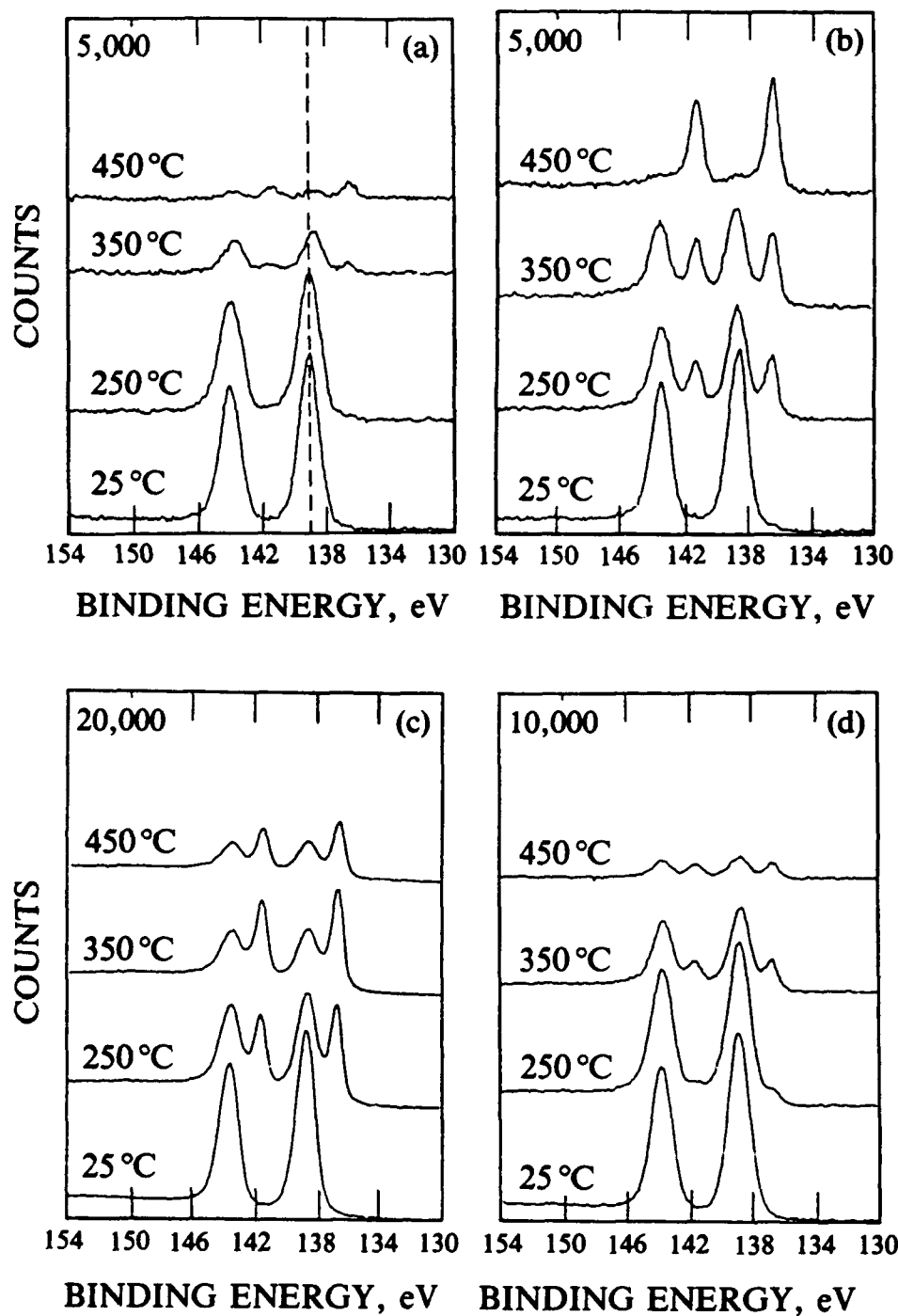


Figure 5. The Pb 4f XPS peaks of Pbnp treated 440C as a function of the sample heating temperatures listed on the figure. The samples are: (a) solvent cleaned, unscratched; (b) solvent cleaned, scratched; (c) acid etched, unscratched; and (d) base washed, unscratched.

#### IV. CONCLUSIONS

The surface chemical composition of 440C steel has been explored and modified by chemical and physical treatments. The layered oxide structure for a sample polished in air with an alumina/water slurry and cleaned with ethanol had an iron oxide layer ~2.5 nm thick and a chromium oxide underlayer ~1.5 nm thick on top of the metallic steel substrate. Beneath the  $\text{Cr}_2\text{O}_3$  layer, the steel had essentially the bulk composition, indicating that the chromium enrichment observed in other studies of high chromium steels is limited to a very narrow region in surfaces treated this way. The chemical composition of 440C can be altered by both physical and chemical means. When the surface is bombarded with  $\text{Ar}^+$  ions, the iron oxide is both sputtered away and chemically reduced to metallic Fe. Etching the surface with HCl removes the iron oxide overlayer but can also cause surface damage by breaching the chromium oxide barrier layer and corroding the bulk steel. The alkaline wash treatment is the most effective at selectively removing the iron oxide overlayer without damaging the surface.

The interactions of sputter deposited  $\text{MoS}_2$  films with the steel surfaces depended on surface pretreatments. The  $\text{MoS}_2$  films had greater adhesion on the chemically pretreated surfaces, indicating stronger bonding between the film and the altered substrate. In addition, the  $\text{MoS}_2$  films were slightly denser, showing a small enhancement of the nucleation process during film growth. Both improved adhesion and densification of films have been shown to increase wear life in rolling contact testing (e.g., ball bearings). It is not clear, however, whether the film properties were enhanced by interacting with the  $\text{Cr}_2\text{O}_3$  underlayer or whether the chemical treatments provided more active sites for film growth.

The effects of surface composition on Pbnp bonding and reactivity are more clearly outlined by this study. Without any pretreatment, the Pbnp physisorbed on the contaminated iron oxide overlayer. On heating, most of the Pbnp present on this surface desorbed, leaving only small amounts of chemisorbed Pbnp and metallic Pb. When the 440C surface was scratched to expose bulk steel to the Pbnp, the additive chemisorbed by breaking C-O bonds in the carboxylate group. On heating, the scratched surface readily formed metallic Pb when metallic Fe was exposed. On both the acid and base treated surfaces, Pbnp chemisorbed in a similar fashion as on the scratched area. On heating, however, the acid etched surface tended to retain more Pb and form metallic Fe and Pb more readily. In contrast, the base treated surfaces, which had the most effective removal of iron oxide, tended to lose most or all of the surface Pb. This indicates that the bonding and reactivity of Pbnp on the  $\text{Cr}_2\text{O}_3$  underlayer is quite weak and that the surface damage done in the acid etching probably created sites for Pbnp reaction. This work suggests that Pbnp provides EP protection by forming a layer of metallic Pb when the oxide layers on asperities are worn away and temperatures increase during boundary contact. Metallic Pb can act as a solid lubricant to provide the protection.

## REFERENCES

1. S. Jin and A. Arens, *Appl. Phys. A.*, **1990**, *50*, 287, and references therein.
2. J. E. Castle, R. Ke, and J. F. Watts, *Corros. Sci.*, **1990**, *30*, 771.
3. W. O. Winer, *Wear*, **1967**, *10*, 422.
4. M. N. Gardos, in *Proceedings of the 16th Leeds-Lyon Symposium on Tribology*, D. Dowson, C. M. Taylor, and M. Godet, eds.; Elsevier: Amsterdam, 1990, p. 2.
5. M. R. Hilton and P. D. Fleischauer, *J. Mater. Res.*, **1990**, *5*, 406, and references therein.
6. P. D. Fleischauer and R. Bauer, *Tribol. Trans.*, **1988**, *31*, 239.
7. M. R. Hilton and P. D. Fleischauer, *Mat. Res. Soc. Symp. Proc.*, **1989**, *140*, 227.
8. S. V. Didziulis and P. D. Fleischauer, *Langmuir*, **1990**, *6*, 621.
9. M. R. Hilton, R. Bauer, S. V. Didziulis, and P. D. Fleischauer, *Thin Solid Films*, **1991**, *201*, 49.
10. H. J. Mathieu and D. Landolt, *Corros. Sci.*, **1986**, *26*, 547.
11. G. Ertl and J. Koppers, *Low Energy Electrons and Surface Chemistry*, 2nd ed.; Verlagsgesellschaft: Weinheim, FRG, 1985, ch. 3.
12. S. Tanuma, C. J. Powell, and D. R. Penn, *Surf. Sci.*, **1987**, *192*, L849.
13. M. P. Seah and W. A. Dench, *Surf. Interf. Anal.*, **1979**, *1*, 2.
14. J. J. Yeh and I. Lindau, *At. Data Nucl. Data Tables*, **1985**, *32*, 1.
15. M. R. Hilton, R. Bauer, and P. D. Fleischauer, *Thin Solid Films*, **1990**, *188*, 219.
16. P. A. Bertrand and P. D. Fleischauer, *J. Vac. Sci. Technol.*, **1980**, *17*, 1309.
17. S. V. Didziulis and P. D. Fleischauer, *Langmuir*, in press.

## TECHNOLOGY OPERATIONS

The Aerospace Corporation functions as an "architect-engineer" for national security programs, specializing in advanced military space systems. The Corporation's Technology Operations supports the effective and timely development and operation of national security systems through scientific research and the application of advanced technology. Vital to the success of the Corporation is the technical staff's wide-ranging expertise and its ability to stay abreast of new technological developments and program support issues associated with rapidly evolving space systems. Contributing capabilities are provided by these individual Technology Centers:

**Electronics Technology Center:** Microelectronics, solid-state device physics, VLSI reliability, compound semiconductors, radiation hardening, data storage technologies, infrared detector devices and testing; electro-optics, quantum electronics, solid-state lasers, optical propagation and communications; cw and pulsed chemical laser development, optical resonators, beam control, atmospheric propagation, and laser effects and countermeasures; atomic frequency standards, applied laser spectroscopy, laser chemistry, laser optoelectronics, phase conjugation and coherent imaging, solar cell physics, battery electrochemistry, battery testing and evaluation.

**Mechanics and Materials Technology Center:** Evaluation and characterization of new materials: metals, alloys, ceramics, polymers and their composites, and new forms of carbon; development and analysis of thin films and deposition techniques; nondestructive evaluation, component failure analysis and reliability; fracture mechanics and stress corrosion; development and evaluation of hardened components; analysis and evaluation of materials at cryogenic and elevated temperatures; launch vehicle and reentry fluid mechanics, heat transfer and flight dynamics; chemical and electric propulsion; spacecraft structural mechanics, spacecraft survivability and vulnerability assessment; contamination, thermal and structural control; high temperature thermomechanics, gas kinetics and radiation; lubrication and surface phenomena.

**Space and Environment Technology Center:** Magnetospheric, auroral and cosmic ray physics, wave-particle interactions, magnetospheric plasma waves; atmospheric and ionospheric physics, density and composition of the upper atmosphere, remote sensing using atmospheric radiation; solar physics, infrared astronomy, infrared signature analysis; effects of solar activity, magnetic storms and nuclear explosions on the earth's atmosphere, ionosphere and magnetosphere; effects of electromagnetic and particulate radiations on space systems; space instrumentation; propellant chemistry, chemical dynamics, environmental chemistry, trace detection; atmospheric chemical reactions, atmospheric optics, light scattering, state-specific chemical reactions and radiative signatures of missile plumes, and sensor out-of-field-of-view rejection.